Journal of Applied Polymer Science

# Tunable Morphology and Photoluminescence of Poly(Styrene-*block*-4-Vinylpyridine)–Cadmium Sulfide Nanocomposites

**Yanmao Dong**[1,2]

[1]School of Chemistry and Bioengineering, Suzhou University of Science and Technology, Suzhou 215009, China

[2]Jiangsu Key Laboratory for Environment Functional Materials, Suzhou University of Science and Technology, Suzhou 215009, China

Correspondence to: Y. Dong (E-mail: dongyanmao@1163.com)

**ABSTRACT:** Poly(styrene-*block*-4-vinylpyridine) (PS4VP)–CdS nanocomposites containing different concentrations of CdS were synthesized by an *in situ* method. Scanning electron microscopy and transmission electron microscopy results indicate that the morphologies of PS4VP–Cd(II) and PS4VP–CdS were controlled by the Cd(II) concentration and the solvent, respectively. The effects of the CdS concentration on the crystal style of CdS in PS4VP–CdS and the photoluminescence (PL) properties of the PS4VP–CdS were also examined. By a comparison of the PL spectra of PS4VP–CdS in solutions, films, and powders, the PL mechanism of PS4VP–CdS was also delivered. The PS4VP–CdS nanocomposite shows potential for application in water-soluble fluorescence probes. © 2012 Wiley Periodicals, Inc. J. Appl. Polym. Sci. 000: 000–000, 2012

**KEYWORDS:** fluorescence; morphology; nanocomposites; optics; self-assembly

Received 26 October 2011; accepted 12 January 2012; published online

**DOI: 10.1002/app.36807**

## INTRODUCTION

Amphiphilic polystyrene (PS)–polyvinylpyridine copolymers have attracted great interest because of their soluble,[1,2] thermoresponsive,[3] and pH-responsive[4] properties and potential uses in electronics, optics, magnetics, catalysts, and sensors. In these applications, composite materials consisting of nanoparticles and organic materials are often adopted to improve these polymer properties. The thermal stability,[5] second-order optical nonlinearity, and electron-tunneling properties of PS–polyvinylpyridine/inorganic nanoparticles composites also have been studied.[6,7] These properties of nanocomposites may depend on the morphology and structure of the polymers and their nanocomposites.[8,9] Therefore, the designed structure of poly(styrene-*block*-4-vinylpyridine) (PS4VP)[10,11] and its nanocomposites were studied recently.[12] Zhao and coworkers[13,14] reported the preparation of CdS nanoparticles within poly(styrene-*block*-2-vinylpyridine) micelles. The size of the CdS nanoparticles were affected by the starting pH value in water, the complex concentration, and the $S^{2-}$ source. PS4VP–CdS nanoparticles have also been modified by mercaptoacetic acid. The CdS nanoparticles induced a morphological transformation in PS4VP from hexagonally packed cylinders to a lamellar structure.[15] However, there is a lack of further discussion on the effect of the concentration and size of CdS on the morphology and photoluminescence (PL) properties of PS4VP–CdS nanocomposites.

In this article, we address the effect of the concentration and size of CdS on the morphology and PL performance of PS4VP–CdS nanocomposites.

## EXPERIMENTAL

### Materials

We used a diblock copolymer of PS and poly(4-vinylpyridine) (P4VP) [PS4VP; P105–styrene-*block*-4-vinylpyridine, with a PS number-average molecular weight ($M_n$) of 21,400 g $mol^{-1}$, a P4VP $M_n$ of 20,700 g/mol, and a weight-average molecular weight/$M_n$ of 1.13, Polymer Source, Inc.]. All other reagents and solvents (obtained from Aldrich or Fluka, Shanghai, China) were used as received.[16]

### Synthesis of PS4VP–Cd(II)

PS4VP–Cd(II) was prepared as follows: Cd $(CH_3COO)_2$ was dissolved in a PS4VP/dimethylformamide (DMF) solution [$Cd(CH_3COO)_2$/4VP = 1: 5–1: 40 mol/mol; PS4VP/DMF = 1: 2 v/v], and the mixture was stirred at room temperature for 3 days. The solid PS4VP–Cd(II) were deposited from the DMF solution by a methanol/water mixture (methanol/water = 1: 1 v/v) was then dried *in vacuo* (at 60°C) overnight.

**Table I.** Dependence of the CdS Concentration in PS4VP–CdS on the Molar Ratio of the Raw Materials

| Sample | PS4VP–CdS-0.08 | PS4VP–CdS-0.6 | PS4VP–CdS-1.2 | PS4VP–CdS-3.4 |
|---|---|---|---|---|
| $Cd(CH_3COO)_2$/4VP (mol/mol) | 1: 40 | 1: 20 | 1: 10 | 1: 5 |
| CdS (wt %) | 0.08 | 0.6 | 1.2 | 3.4 |

### Preparation of PS4VP–CdS

The solid PS4VP–Cd(II) was dissolved in a DMF/water solution (DMF/water = 100: 1 v/v), and then, PS4VP–Cd(II) was reacted with 0.1 mol/L $Na_2S$ ($Cd/S^{2-}$ = 1: 1 mol/mol) in 50 mL of a DMF solution at 25°C for 1 h. The solution was dispersed by ultrasound (300 W) for 1 h. The solid nanocomposites were deposited from the DMF solution by a methanol/water mixture (methanol/water = 1: 1 v/v), and then, the obtained PS4VP–CdS was washed with distilled water and dried *in vacuo* (60°C) for 12 h. The obtained PS4VP–CdS was dissolved in DMF to make a solution, spin-coated (600r/min) to make films, or dried to make powders. The PL spectra were examined at room temperature.

### Instrumentation

$^1$H-NMR spectra were recorded in dimethyl sulfoxide on an Inova-400 instrument with tetra-order methylsilane as a reference. The CdS concentration in these composites was investigated by means of inductively coupled plasma (PLA-SPECI, Leeman Co.) and a Hitachi S-570 scanning electron microscope equipped with an energy-dispersive X-ray spectroscopy facility. We prepared the samples for inductively coupled plasma by dispersing the product in 98% $HNO_3$ and then boiling it for 30 min. The solution containing Cd was diluted with distilled water. The stability of these complexes were investigated by means of differential scanning calorimetry with a TA Instruments DSC 2010. The samples were examined at a scanning rate of 10 K/min by the application of two heating cycles and one cooling cycle. The morphology and selected area electron diffraction (SAED) pattern of the nanoparticles and composites were determined by scanning electron microscopy (SEM) and a Hitachi H-600-II transmission electron microscope. The solid samples were dissolved in DMF to make a 0.1 g/L solution. Then, 0.1 mL of solution was spread on the carbon support film for transmission electron microscopy (TEM). The *z*-average size and polydispersity index of the nanocomposites were measured by a Malvern HPP 5001 high-performance particle sizer (HPPS) at 25°C. The X-ray diffraction (XRD) patterns were recorded on a Rigaku D/MAX-IIIC X-ray diffractometer with Cu Kα radiation (wavelength ($\lambda$) = 0.1542 nm) operated at 50 kV and 100 mA, with the diffraction angle in the range 2θ = 5–70°. Ultraviolet–visible (UV–vis) absorption spectroscopy of the samples was recorded on a Shimadzu UV–vis spectrophotometer (UV-2401PC) with a scanning range of 190–700 nm. Absorption from the solvent was subtracted from each spectrum. The PL spectra of the products were obtained on an Shimadzu Edinburgh-920 spectrophotometer equipped with a 450-W Xe arc lamp and a photomultiplier tube (PMT) detector at room temperature.

## RESULTS AND DISCUSSION

### Fabrication and Characterizations of the Target Nanocomposites

The CdS concentration in PS4VP–CdS increased from 0.08 to 3.4 wt % as the Cd $(CH_3COO)_2$-to-4VP ratio increased from 1: 40 to 1: 5 (Table I).

The XRD patterns of bulk CdS (powder), PS4VP–Cd(II), and PS4VP–CdS with different CdS concentrations are shown in Figure 1. The diffraction peaks at 2θ = 19.06° [Figure 1(b–e)] corresponded to amorphous PS4VP. The XRD pattern of bulk CdS [Figure 1(a)] and PS4VP–CdS [Figure 1(d,e)] indicate both the cubic and hexagonal CdS crystal structure for the nanoparticles.[17] However, there were only cubic [Figure 1(c)] and hexagonal [Figure 1(f)] CdS crystallites in the PS4VP–CdS nanocomposites, containing 0.08 and 3.4 wt % CdS, respectively. These results indicate that the CdS with a hexagonal phase was gradually replaced with the CdS with a mixed phase of cubic and hexagonal as the CdS concentration increased. The crystallinity transformation may have been driven by the thermodynamics stability because the hexagonal CdS was more stable than the cubic CdS. The change in the Cd-to-S ratio also affected the CdS crystal style.[18]

The average diameter of CdS particles was estimated according to the Debye–Scherer equation:[19]

$$L_{hkl} = k\lambda/(B\cos\theta)$$

where $L_{hkb}$ is the crystallite size; $k$, the Scherrer constant; $B$, the half-width of the diffraction peak (radians); $\theta$, the diffraction angle, $k$ is taken as 1, $\lambda$ = 0.15418 nm, and $B$ is the half-width of the diffraction peak (radians). The size of CdS increased from about 1.3 nm [Figure 1(a)] and 5.3 nm [Figure 1(e)] to 32 nm [Figure 1(f)]. This indicated that the CdS nanoparticles congregated together as the CdS concentration increased.

### Dependence of the Morphology of PS4VP–Cd(II) and PS4VP–CdS on the Cd(II) (CdS) Concentration

Figure 2 shows the morphological change of PS4VP–Cd(II) with different Cd(II) concentrations dispersed in DMF. It

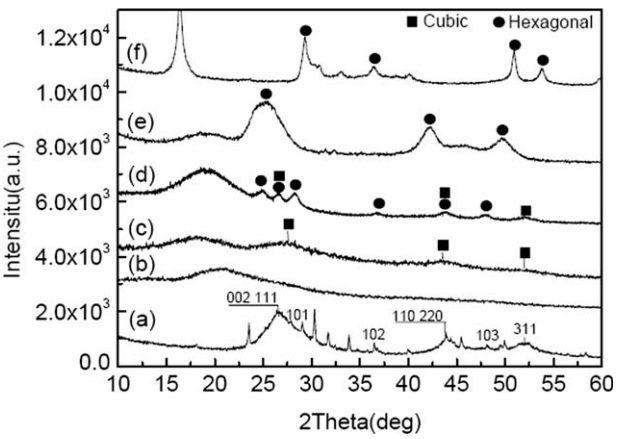


**Figure 1.** XRD patterns of the samples: (a) CdS, (b) PS4VP, (c) PS4VP–CdS-0.08, (d) PS4VP–CdS-0.6, (e) PS4VP–CdS-1.2, and (e) PS4VP–CdS-3.4.

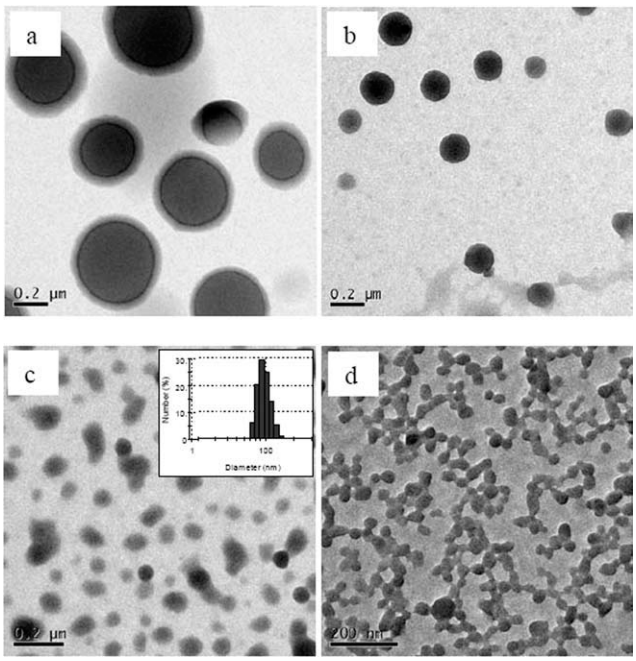


**Figure 2.** Dependence of the PS4VP–Cd(II) morphology by TEM measurement on the Cd(II) concentration: (a) PS4VP–Cd(II)-0.08, (b) PS4VP–Cd(II)-0.6, (c) PS4VP–Cd(II)-1.2, and (d) PS4VP–Cd(II)-3.4. DMF was used as a solvent. The inset in image c shows the dispersability of the nanocomposites by HPPS measurement.

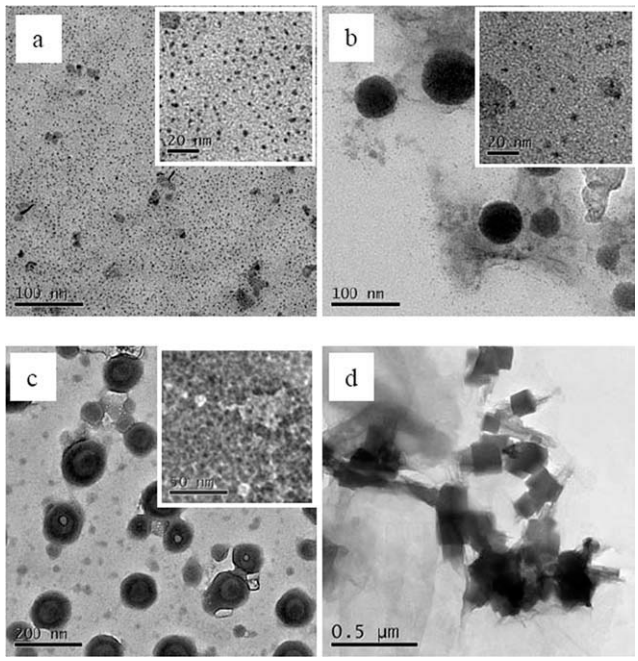


**Figure 3.** Dependence of the morphology of the CdS and PS4VP–CdS nanocomposites on the CdS concentration: (a) PS4VP–CdS-0.08, (b) PS4VP–CdS-0.6, (c) PS4VP–CdS-1.2, and (d) PS4VP–CdS-3.4. The insets show magnified images of the CdS particles. Water was used as the solvent.

indicates that the PS4VP–Cd(II) with low Cd(II) concentration tended to form nanospheres [Figure 2(a,b)]. As the Cd(II) concentration increased, the PS4VP–Cd(II) particles congregated together and self-assembled to nanodumbbells, even wormlike shapes. The particle size also decreased from about 500 nm to about 50 nm [Figure 2(c,d)]. These changes could be attributed to the strong interaction between polymer chains, which resulted from the 4VP–Cd(II) groups (Scheme 1). This indicated that the morphology of the PS4VP–Cd(II) could be controlled by the adjustment of the Cd(II) concentration.[20]

The structure of nanocomposites was also studied by TEM measurement (Figure 3). The average size of the CdS nanocrystals was about 3–4 nm, as shown in Figure 3(a); this was larger than that calculated from XRD (~2.3 nm). The difference may have been due to some aggregation of the CdS nanocrystals. The data calculated from XRD results reflected the size of a single crystal, whereas the TEM photograph shows the aggregates of the CdS particles. This may have been due to the high surface energy of the nanometer-sized crystals. As the CdS concentration increased, as shown in Figure 3(b–d), the CdS particles congregated together. The size of the nanocrystal varied from about 5–8 nm to about 150 nm. This indicated that the morphology of the PS4VP–CdS and the size of the CdS nanoparticles could be controlled by the adjustment of the concentration of CdS.[21]

To clarify the agglomeration of the CdS nanoparticles in PS4VP–CdS, the PS4VP–CdS containing 0.08 and 3.4 wt % CdS were dispersed in DMF. Then, the solutions were dropped onto the glass surface. The morphology of the films were studied by SEM measurement. As shown in Figure 4, PS4VP–CdS was monodisperse. Separate CdS crystallites are shown in Figure 4(b) (3.4 wt % CdS). These could be assigned to the strong interactions between the CdS nanoparticles and PS4VP chains (Scheme 2).[22]

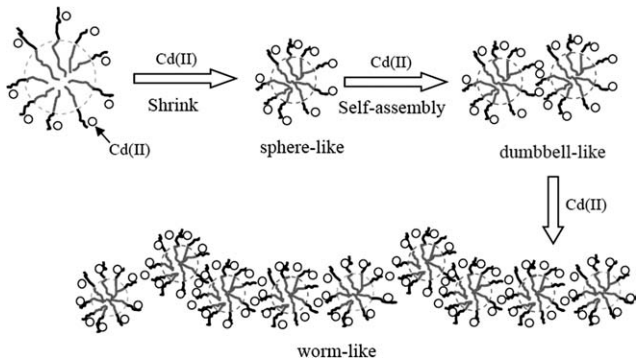


**Scheme 1.** Schematic chart to explain the dependence of the morphology of PS4VP–Cd(II) on the Cd(II) concentration

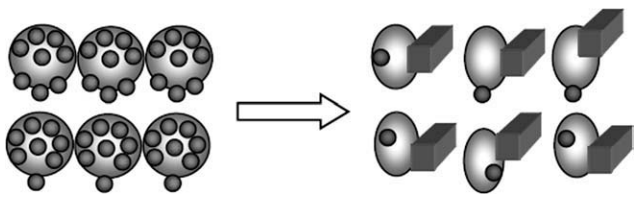

**Scheme 2.** Schematic chart to form the separate CdS crystallite from PS4VP–CdS.

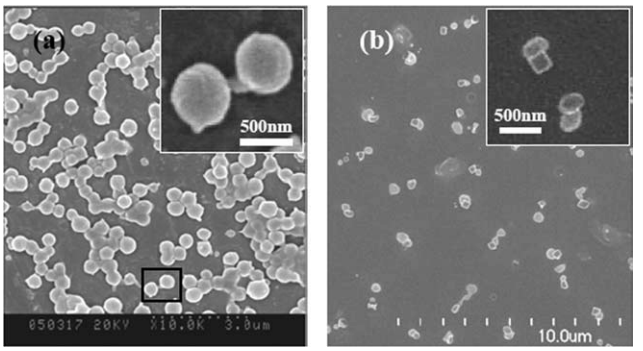


**Figure 4.** SEM micrograph of PS4VP–CdS with (a) 0.08 and (B) 3.4 wt % CdS. DMF was used as the solvent.

Further insight into the structures of the CdS nanoparticles in the nanocomposites was obtained with SAED measurement. The SAED rings of the PS4VP–CdS revealed the formation of single crystals. According to the formula $d = (L\lambda)/R$, where $R$ is radius of the diffraction ring, $L$ (=800 mm) is a constant of the camera, and $\lambda$ is the wavelength of an electron ($\lambda = 0.0037$ nm, 100 kV), the $d$-spacing calculated from Figure 5 corresponded to the lattice planes (111), (220), and (311) for cubic CdS [Figure 5(a)], cubic/hexagonal CdS [Figure 5(b,c)], and hexagonal CdS [Figure 5(d)], respectively; this was in agreement with the XRD results.[23] This indicated that the crystal style of CdS in the PS4VP–CdS was controllable.[24]

### Dependence of the Morphology of PS4VP–CdS on the Solvent by SEM Measurement

It has been demonstrated that there are nucleation and growth stages in the preparation of one-dimensional (1D) nanostructures.[25] Homogeneous nucleation, heterogeneous nucleation, and secondary nucleation are the characteristic nucleation processes. During the formation of 1D nanostructures, the interaction between nanoparticles and interfaces and also the chemical properties of the solution affect the structure of 1D materials. In this work, heterogeneous nucleation and size reduction played important roles in the formation of the PS4VP–CdS microstructures. To determine the effect of the solvent on the structure, PS4VP–CdS-3.4 (where the number indicates the weight percentage of CdS) was resolved in methanol, ethanol, *n*-propanol, and *n*-butanol, respectively. The PS4VP–CdS-3.4 solution was dropped on the glass and dried at room temperature. As shown in Figure 6, the nanocomposites were shaped as nanofilms [Figure 6(a)], nanowires [Figure 6(b)], nanorods [Figure 6(c)], and nanoholes [Figure 6(d)]. These were assigned to the different evaporation rates, polarities, and surface tensions of the solvents. By comparison, the evaporate rate of solvents were as follows: as *n*-Butanol (117°C) < *n*-Propanol (98°C) < Ethanol (78°C) < Methanol (65°C); this was the reverse order of surface tension, that is, *n*-Butanol (27.18 dyn/cm) > *n*-Propanol (25.26 dyn/cm) > Ethanol (24.05 dyn/cm) > Methanol (22.00 dyn/cm). When the solvent was evaporated quickly, the nanocomposites were formed films of the original shape [Scheme 3(a)]. As the evaporation rate decreased and the surface tension increased, the size reduction rate of PS4VP–CdS along the radial was slower than that along the axis; hence, the nanocomposites were shaped as nanowires or nanorods [Scheme 3(b)]. Compared to *n*-propanol, ethanol, and methanol, *n*-butanol had the slowest evaporate rate and the strongest surface tension, so the PS4VP–CdS-3.4 congregated along both the radial and the axis to form the nanoholes [Scheme 3(c)]. This indicated that the microstructures of PS4VP–CdS could be controlled with different solvents.[26,27]

### Dependence of the Absorption Apectra of PS4VP–CdS on the CdS Concentration

The UV–vis absorption spectra of PS4VP–CdS (containing 0.08, 0.6, 1.2, and 3.4 wt % CdS) in Figure 7 showed the absorption edge. The UV thresholds of samples a, b, c, and d were observed at 290, 300, 310, and 325 nm, respectively; this corresponded to to band gaps of 4.28, 4.13, 4.00, and 3.82 eV. These values revealed that the growth mechanism of the CdS nanoparticles was Ostwald ripening; that is, the particles grew by the formation of bonds between the source ions and surface atoms, with the particles continually enlarging and the wavelength of the onset of absorption continually increasing.[28] This indicated that the absorption spectra microstructures of PS4VP–CdS could be controlled by the CdS concentration.

### Dependence of the PL Properties of P4VP–CdS on the CdS Concentration and Size

The CdS nanoparticles in PS4VP–CdS affected the PL properties of the PS4VP–CdS nanocomposites. As shown in Figure 8, the PL intensity of the PS4VP–CdS solution was stronger than that of PS4VP–Cd(II). The fluorescence efficiency (FE; $\phi$) was obtained by a method mentioned in literature.[29] The results show that $FE_{PS4VP–CdS}$ (0.23) > $FE_{PS4VP–Cd(II)}$ (0.18); this could be attributed to the volume effect and surface effect of nano-CdS. The marked peaks of PS4VP–CdS redshifted from 357, 393, 402, to 437 nm; this corresponded to PS4VP–CdS-0.08 (excited wavelength ($\lambda_{ex}$) = 285 nm), PS4VP–CdS-0.6 ($\lambda_{ex}$ = 324 nm), PS4VP–CdS-1.2 ($\lambda_{ex}$ =

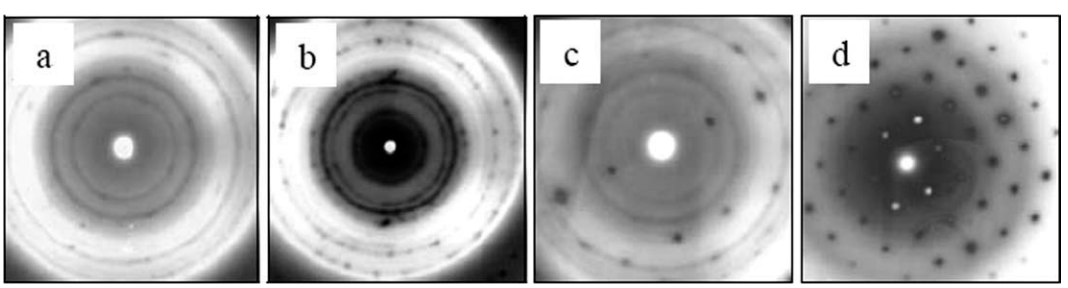


**Figure 5.** SAED images of the PS4VP–CdS nanocomposites: (a) PS4VP–CdS-0.06, (b) PS4VP–CdS-0.6, (c) PS4VP–CdS-1.2, and (d) PS4VP–CdS-3.4.

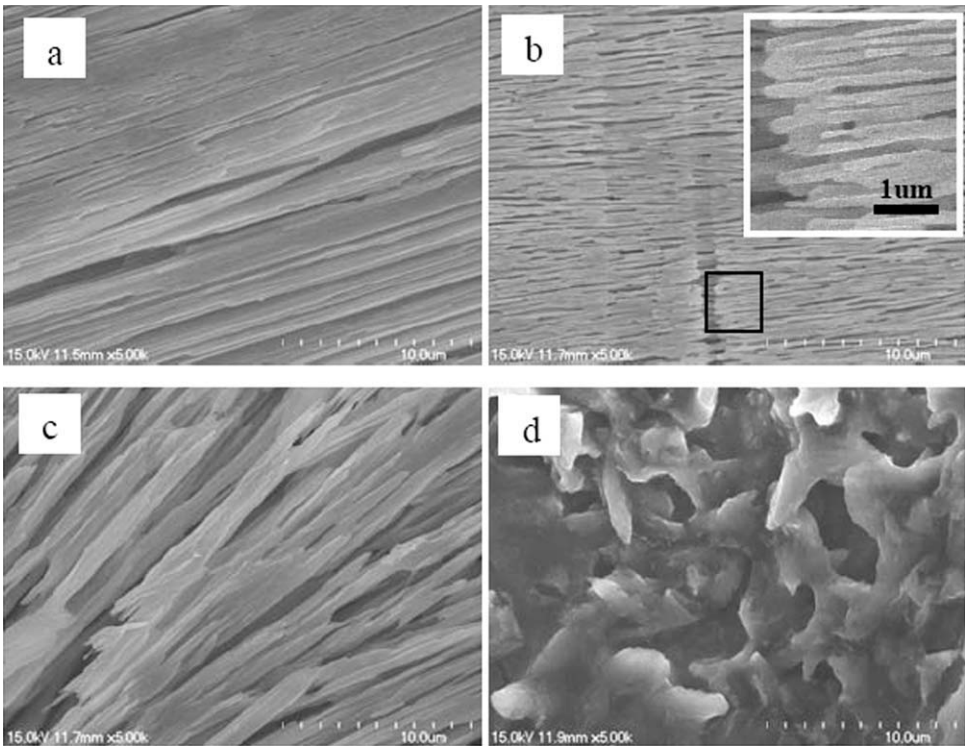


**Figure 6.** SEM micrograph of PS4VP–CdS-3.4 with different solvents: (a) methanol, (b) ethanol, (c) *n*-propanol, and (d) *n*-butanol.

326 nm), and PS4VP–CdS-3.4 ($\lambda_{ex}$ = 373 nm), respectively, and indicated that the size of the CdS particles increased with increasing CdS concentration. As a result, the size and surface states of the CdS nanoparticles tuned the PL of PS4VP–CdS.[30]

Figure 9 compares the PL properties of the PS4VP–CdS films with different concentrations of CdS. The marked peaks of PS4VP–CdS were located at 365 nm [emission of PS4VP–Cd(II)] and 515 nm (emission of CdS), respectively. The PL intensity of PS4VP–CdS increased with increasing CdS concentration, both in the PS4VP–Cd(II) and CdS positions. The slight redshift of the PS4VP–CdS emission from Figure 9(a) to Figure 9(d) was also observed; this indicated the growth of CdS particles. The aggregation of CdS nanoparticles and the coplane structure of the PS4VP/CdS film were responsible for the redshift (from 437 to 515 nm) of the fluorescence emission compared with that of the PS4VP/CdS solution.[31]

Figure 10 compares the PL properties of the PS4VP–CdS powders with different concentrations of CdS. The marked peaks of PS4VP–Cd(II) and CdS were located at 346 and 586 nm, respectively. The marked peaks of PS4VP–CdS redshifted from 551 to 652 nm; this corresponded to PS4VP–CdS-3.4 ($\lambda_{ex}$ = 396 nm) and PS4VP–CdS-23.4 ($\lambda_{ex}$ = 400 nm), respectively, and indicated that the CdS particles congregated as the CdS

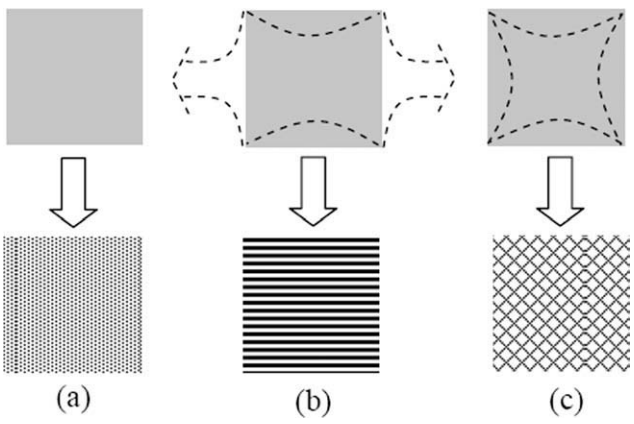


**Scheme 3.** Schematic chart to form the tunable morphology of PS4VP–CdS: (a) film, (b) nanowire or nanorod, and (c) nanohole.

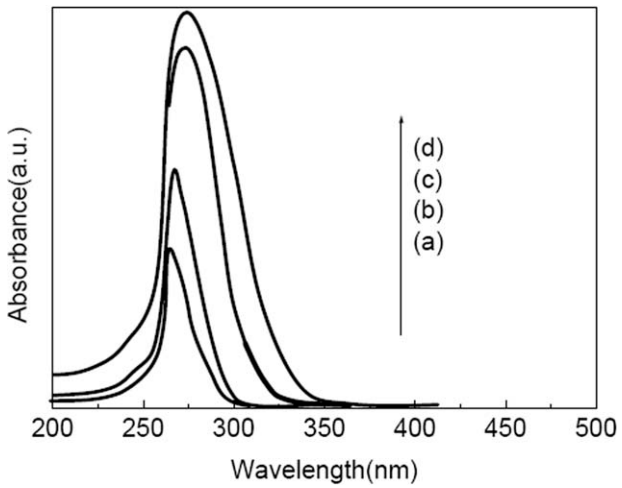


**Figure 7.** UV–vis absorption spectra of (a) PS4VP–CdS-0.08, (b) PS4VP–CdS-0.6, (c) PS4VP–CdS-1.2, and (d) PS4VP–CdS-3.4 (0.6 g/L DMF solution).

Applied Polymer SCIENCE

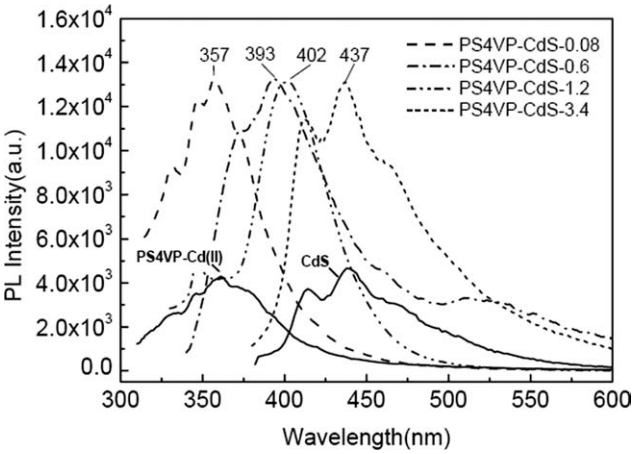


**Figure 8.** PL spectra of PS4VP–Cd(II), PS4VP–CdS-0.08 ($\lambda_{ex}$ = 285 nm), PS4VP–CdS-0.6 ($\lambda_{ex}$ = 324 nm), PS4VP–CdS-1.2 ($\lambda_{ex}$ = 326 nm), and PS4VP–CdS-3.4 ($\lambda_{ex}$ = 373 nm, 0.6 g/L DMF solution). For comparative analysis, the PL intensities of the different PS4VP–CdS were evened up.

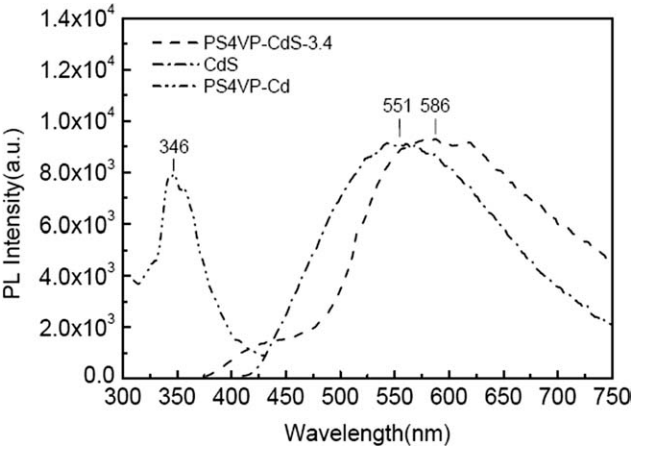


**Figure 10.** PL spectra of the powders: PS4VP–Cd(II) ($\lambda_{ex}$ = 295 nm), CdS ($\lambda_{ex}$ = 348 nm), PS4VP–CdS-3.4 ($\lambda_{ex}$ = 396 nm), and PS4VP–CdS-23.4 (23.4 wt % CdS, $\lambda_{ex}$ = 400 nm).

concentration increased. Nonradiative energy transfer existed between the PS4VP and CdS nanoparticles in PS4VP–CdS-23.4. This indicated that the PL spectra of PS4VP–CdS was controllable by the CdS concentration.

As shown by a comparison of the curves in Figures 8–10, the characteristic emission peaks of PS4VP–CdS belonged to both the PS4VP and CdS nanoparticles. A PS4VP-to–CdS PL transformation was also observed. To discuss the PL mechanism of PS4VP–CdS, a schematic illustration of the energy band profiles of the PS4VP–CdS nanocomposites and the routes for excitation and charge transfer are shown in Scheme 4. The valence band (VB) offset (~2.0 eV) was smaller than the conduction band (CB) offset (~4.0 eV), and the electron-hole recombination occurring in the CdS nanoparticles was dominant. When photons were absorbed, electrons were excited into the lowest unoccupied molecular orbital of the pyridine groups in PS4VP, and holes were left in the highest occupied molecular orbital. The excited electrons in the PS4VP–CdS nanocomposites chose to migrate from PS4VP to the CdS nanoparticles. However, because of the low concentration of CdS in the nanocomposites, the excited electrons mainly returned from the CB back to the VB through a radiative process. Consequently, the PS4VP–CdS showed emission from both the nanocrystal and the polymer because of the electron-hole recombination in both components.[32,33] The larger Stokes shift of PS4VP–CdS (~152–252 nm) compared to that of PS4VP–Cd(II) were assigned to the quantum effect from CdS nanoparticles. In conclusion, the

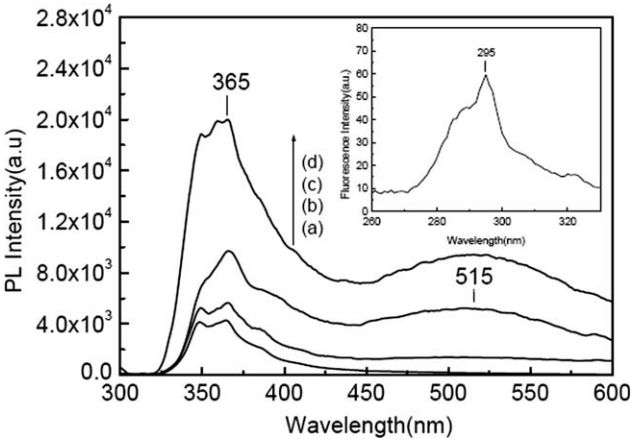


**Figure 9.** PL spectra of the PS4VP–CdS films: (a) PS4VP–CdS-0.08, (b) PS4VP–CdS— 0.6, (c) PS4VP–CdS-1.2, and (d) PS4VP–CdS-3.4 ($\lambda_{ex}$ = 295 nm).

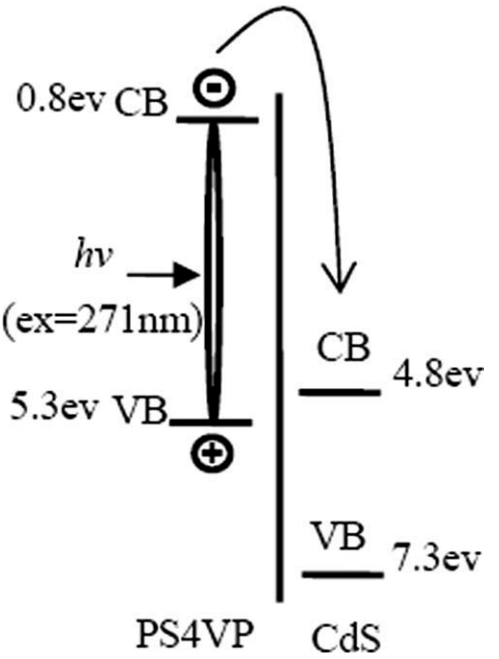


**Scheme 4.** Schematic illustration of the energy band profiles of the chemically derivatized PS4VP–CdS nanocomposites and the routes for excitation and charge transfer. The band positions of the CdS nanoparticles were estimated on the basis of the electron binding energies as measured by VB photoemission. The curved arrows indicate the direction of carrier transfer. *hv* = Light.

nonradiative or radiative energy transfer in PS4VP–CdS may have been controlled by the CdS concentration.

## CONCLUSIONS

This work demonstrates the morphological changes of PS4VP–CdS nanocomposites by the solvent and the CdS concentration. The CdS concentration also affected the PL properties of the nanocomposites. The PS4VP–CdS nanocomposite showed potential for application in water-soluble fluorescence probes.

## ACKNOWLEDGMENTS

The authors thank the Priority Academic Program Development of Jiangsu (China) Higher Education Institutions (PAPD) for financial support.

## REFERENCES

1. Kee, R. A.; Gauthier, M. *Macromolecules* **2002,** *35*, 6526.
2. Njikang, G.; Gauthier, M.; Li, J. *Polymer* **2008,** *49*, 1276.
3. Raula, J.; Shan, J.; Nuopponen, M.; Niskanen, A.; Jiang, H.; Kauppinen, E. I.; Tenhu, H. *Langmuir* **2003,** *19*, 3499.
4. Li, D.; He, Q.; Cui, Y.; Li, J. *Chem. Mater.* **2007,** *19*, 412.
5. Zhang, B. Q.; Chen, G. D.; Pan, C. Y.; Luan, B.; Hong, C. Y. *J. Appl. Polym. Sci.* **2006,** *102*, 1950.
6. Li, C. P.; Wei. K. H.; Yi, J. Angew, H. *Angew. Chem. Int. Ed.* **2006,** *5*, 1449.
7. Zhang, Y.; Ma, M.; Wang, X.; Fu, D.; Zhang, H.; Gu, N.; Liu, J.; Lu, Z.; Xu, L.; Chen, K. *J. Phys. Chem. Solids* **2003,** *64*, 927.
8. Vaia, R. A.; Maguire, J. F. *Chem. Mater.* **2007,** *19*, 2736.
9. Wu, K. J.; Chu, K. C.; Chao, C. Y.; Chen, Y. F.; Lai, C. W.; Kang, C. C.; Chen, C. Y.; Chou, P. T. *Nano. Letter* **2007,** *7*, 1908.
10. Yuan, J. J.; Ma, R.; Gao, Q.; Wang, Y. F.; Cheng, S. Y.; Feng, L. X.; Fan, Z. Q.; Jiang, L. *Appl. Polym. Sci.* **2003,** *89*, 1017.
11. Zheng, G.; Pan, C. *Macromolecules* **2006,** *39*, 95.
12. Hayward, R. C.; Chmelka, B. F.; Kramer, E. J. *Adv Mater* **2005,** *17*, 2591.
13. Zhao, H.; Douglas, E. P. *Chem. Mater.* **2002,** *14*, 1418.
14. Zhao, H.; Douglas, E. P.; Harrison, B. S.; Schanze, K. S. *Langmuir* **2001,** *17*, 8428.
15. Yeh, S. W.; Wei, K. H.; Sun, Y. S.; Jeng, U. S.; Liang, K. S. *Macromolecules* **2005,** *38*, 6559.
16. Arzu, T.; Sevgi, B. *J Mol Struct* **2001,** *595*, 93
17. Badr, Y.; Abd, El-Kader, K.; Khafagy, R. *J. Appl. Polym. Sci.* **2004,** *92*, 1984.
18. Orimia, R. L.; Shahtahmasebia, N.; Tajabora, N.; Kompany, A. *Physica. E.* **2008,** *40*, 2894.
19. Wang, S.; Yang, S.; Yang, C.; Li, Z.; Wang, J.; Ge, W. *J. Phys. Chem. B.* **2000,** *104*, 11853.
20. Choi, M.; Chung, B.; Chun, B.; Chang, T. *Macromol. Res.* **2004,** *12*, 127.
21. Gilman, E. S.; Toombes, A. C.; Finnefrock, M. W.; Tate, R. U.; Ulrich, W.; Sol, M. G. *Macromolecules* **2007,** *40*, 8974
22. Yeh, S.; Carrot, G.; Scholz, S.; Plummer, C. *J. Chem. Mater.* **1999,** *11*, 3571.
23. Christopher, M.; Daniel, M.; Ding, Y.; Li, J.; Wang, Z. *Int. J. Nanotechnol.* **2004,** *1*, 231.
24. Piñeiro, Á.; Brocos, P.; Amigo, A.; Gracia-Fadrique, J. *Fluid Phase Equilib.* **2004,** *225*, 115.
25. Xia, Y.; Yang, P.; Sun, Y.; Wu, Y.; Mayers, B.; Gates, B.; Yin, Y.; Kim, F.; Yan, H. *Adv. Mater.* **2003,** *15*, 353.
26. Gates, B.; Xu, Q.; Stewart, M.; Ryan, D.; C.; Willson, G.; Whitesides, G. *Chem. Rev.* **2005,** *105*, 1171.
27. Kim, G.; Wutzler, A.; Radusch, H.; Michler, G.; Simon, P.; Sperling, R.; Parak, W. *Chem. Mater.* **2005,** *17*, 4949.
28. Cumberland, S. L.; Hanif, K. M.; Javier, A.; Khitrov, G. A.; Strouse, G. F.; Woessner, S. M.; Yun, C. S. *Chem. Mater.* **2002,** *14*, 1576.
29. Carrot, G.; Scholz, S. M.; Plummer, C. J. G.; Hilborn, J. G. *Chem. Mater.* **1999,** *11*, 3571.
30. Nair, P. S.; Radhakrishnan, T.; Revaprasadu, N.; Kolawole, G. A.; Brien, P. O. *Polyhedron* **2003,** *22*, 3129.
31. Jin-Long, C.; Chang-Qing, Z. *Anal. Chim. Acta.* **2005,** *546*, 147.
32. Wang, S.; Yang, S.; Yang, C. *J. Phys. Chem. B* **2000,** *104*, 11853.
33. Yang, H.; Holloway, P. *J. Phys. Chem. B* **2003,** *107*, 9705.